

LYMAN α RESONANT SCATTERING IN YOUNG GALAXIES — PREDICTIONS FROM COSMOLOGICAL SIMULATIONS

PETER LAURSEN¹ AND JESPER SOMMER-LARSEN^{1,2}

Draft version July 6, 2018

ABSTRACT

We present results obtained with a three-dimensional, Ly α radiative transfer code applied to a fully cosmological galaxy formation simulation. The developed Monte Carlo code is capable of treating an arbitrary distribution of source Ly α emission, neutral hydrogen density, temperature, and peculiar velocity of the interstellar medium. We investigate the influence of resonant scattering on the appearance and properties of young galaxies by applying the code to a simulated “Lyman-break galaxy” at redshift $z = 3.6$, and of star formation rate $22 M_{\odot} \text{ yr}^{-1}$ and total Ly α luminosity $2.0 \times 10^{43} \text{ erg s}^{-1}$. It is found that resonant scattering of Ly α radiation can explain that young galaxies are frequently observed to be more extended on the sky in Ly α than in the optical. Moreover, it is shown that, for the system investigated, due to the anisotropic escape of the photons, the observed maximum surface brightness can differ by more than an order of magnitude, and the total derived luminosity by a factor of ~ 4 , depending on the orientation of the system relative to the observer.

Subject headings: galaxies: formation — line: formation — line: profiles — radiative transfer — scattering

1. INTRODUCTION

The Ly α line is a very important diagnostic in a wide range of fields of astrophysics, not the least of which is galaxy formation, providing us with extensive information on redshift, dynamics, kinematics, morphology, etc. Three distinct physical processes result in Ly α source emission in the context of galaxies: First, Ly α emission due to photo-ionization of hydrogen atoms by UV radiation from nearby, massive stars and subsequent recombinations may contribute as much as 10% of the total luminosity of the galaxy (Partridge & Peebles 1967). Second, part of the potential energy gained by gas falling into galactic potential wells is converted into cooling radiation. Fardal et al. (2001) find that, at high redshifts, most of this radiation is emitted by gas with $T < 20\,000 \text{ K}$, and consequently $\sim 50\%$ in Ly α alone. Finally, the external, metagalactic UV field, penetrating some (in case of damped Ly α systems) or all (in case of Lyman-limit systems) of the outer parts of galactic hydrogen “envelopes” will also produce some Ly α radiation through case B recombination. Moreover, this UV field can also photo-heat non-self-shielded gas, which subsequently cools, radiating Ly α (Furlanetto et al. 2005).

Over the past years it has become possible to actually resolve observationally these young, Ly α emitting galaxies. In several cases, the galaxies have been found to be significantly more extended on the sky when observed in Ly α as opposed to optical bands (e.g., Møller & Warren 1998; Fynbo et al. 2001, 2003). Due to the complexity and diversity of the systems, in order to correctly interpret observations and make predictions about the properties of young galaxies, it is desirable to develop realistic

theoretical and numerical models.

For a number of idealized cases analytical solution are obtainable. Harrington (1973) investigated the emergent spectrum of resonantly scattered radiation in the case of a highly optically thick slab of finite thickness but infinite extension, and uniform temperature and density. Neufeld (1990) extended this solution to include the possibility of the photons being destroyed (as by dust) and injected with arbitrary initial frequency. Dijkstra et al. (2006) derived a similar analytical expression for spherical symmetry, allowing for isotropic expansion or collapse of the gas, and Loeb & Rybicki (1999) examined the spectrum for an isotropically expanding or contracting medium with no thermal motion.

However idealized these configurations may seem, they provide valuable and at least qualitative insight into the characteristics of young galaxies. Moreover, they offer direct means of testing numerical methods.

The Monte Carlo (MC) method has been used for solving radiative transfer (RT) problems since the beginning of the 1960s. Nevertheless, though conceptually simple, the demand for strong computer power until quite recently restricted this technique to deal with more or less the same idealized configurations that had already been dealt with analytically. Thus, the majority of previous attempts to model RT in astrophysical situations have been based on strongly simplified configurations of the physical parameters. Only a few authors (Cantalupo et al. 2005; Tasitsiomi 2006; Verhamme et al. 2006) considered more general cases.

With the aim of predicting the appearance and properties of Ly α emitting galaxies, we developed an MC code capable of treating an arbitrary distribution of source Ly α emission, neutral hydrogen density, temperature, and peculiar velocity of the medium and subsequently applied it to a simulated Lyman-break galaxy (LBG) from a fully cosmological simulation.

Electronic address: pela@dark-cosmology.dk, jslarsen@tac.dk

¹ Dark Cosmology Centre, Niels Bohr Institute, University of Copenhagen, Juliane Maries Vej 30, DK-2100, Copenhagen Ø, Denmark.

² Institute of Astronomy, University of Tokyo, Osawa 2-21-1, Mitaka, Tokyo, 181-0015, Japan.

2. SIMULATIONS

2.1. The Cosmological Simulation and Monte Carlo Code

The cosmological simulation of the formation and evolution of an individual galaxy was performed using the N-body/hydrodynamical TreeSPH code of Sommer-Larsen et al. (2003, see also Sommer-Larsen (2006)). The system becomes a Milky Way/M31-like disk galaxy at $z = 0$ and is simulated using $\sim 2.2 \times 10^6$ particles in total, comprising only smoothed particle hydrodynamic (SPH) and dark matter (DM) particles at the initial redshift $z_i = 39$. The masses and gravity softening lengths of SPH and star particles are $9.9 \times 10^4 h^{-1} M_\odot$ and $200 h^{-1}$ pc, respectively ($h = 0.65$). For the DM particles the corresponding values are $5.7 \times 10^5 h^{-1} M_\odot$ and $370 h^{-1}$ pc. The minimum SPH smoothing length in the simulation is about $13 h^{-1}$ pc. For the purposes of the present study, a single simulation output, at $z = 3.6$, was chosen.

The MC code, used to propagate the photons through the medium, by and large resembles those recently developed by other authors (e.g., Cantalupo et al. 2005; Tasitsiomi 2006). Since it is grid-based — the number of cells typically being 512^3 — the physical parameters of interest are first interpolated from the SPH particles to the cells of the computational box. These parameters are the Ly α emissivity, the temperature T , the density $n_{\text{H I}}$ of neutral hydrogen, and the three-dimensional velocity field \mathbf{v}_{bulk} of the gas.

2.2. Determination of Source Ly α Emission

The emission cell of a given Ly α photon is found by setting the probability of being emitted from a given cell equal to the ratio of the luminosity in that cell to the total luminosity L_{tot} . The photon is then injected in the line center (in the reference frame of the fluid element) from a random point \mathbf{x}_i in the cell. The frequency ν of the photon is parametrized through $x = (\nu - \nu_0)/\Delta\nu_{\text{D}}$, where $\nu_0 = 2.466 \times 10^{15}$ Hz is the line center frequency and $\Delta\nu_{\text{D}} = (v_{\text{th}}/c)\nu_0$ is the Doppler frequency, with $v_{\text{th}} = (2k_{\text{B}}T/m_{\text{H}})^{1/2}$ being the thermal atom velocity dispersion (times $\sqrt{2}$) and the rest of the variables having their usual meanings. In terms of this variable the injected photon obviously has a frequency of $x = 0$. The initial direction $\hat{\mathbf{n}}_i$ of the photon follows an isotropic probability distribution.

2.3. Propagation of the Radiation

The optical depth τ covered by the photon before it is scattered is drawn randomly from the probability distribution $e^{-\tau}$, and subsequently converted into a physical distance $r = \tau/n_{\text{H I}}\sigma_x$, where the physical parameters are given by the present cell. The cross section σ_x is given by a Voigt profile, i.e. the convolution of the Lorentzian natural line profile and the Gaussian thermal broadening of the atoms, resulting in

$$\sigma_x = f_{12} \frac{\sqrt{\pi} e^2}{m_e c \Delta\nu_{\text{D}}} H(a, x), \quad (1)$$

where $f_{12} = 0.4162$ is the Ly α oscillator strength, and

$$H(a, x) = \frac{a}{\pi} \int_{-\infty}^{+\infty} \frac{e^{-y^2}}{(x-y)^2 + a^2} dy \quad (2)$$

is the Voigt function with $a = \Delta\nu_{\text{L}}/2\Delta\nu_{\text{D}}$ the ratio between the natural line width $\Delta\nu_{\text{L}} = 9.936 \times 10^7$ Hz and the Doppler width. Since eq. (2) is not analytically integrable, we use the analytic fit given by Tasitsiomi (2006).

If the final position \mathbf{x}_f of the photon is outside the original cell, the photon is placed at the point \mathbf{x}_{int} of intersection with the face of the cell and the above calculation is redone with the parameters of the new cell, an optical depth $\tau' = \tau - |\mathbf{x}_{\text{int}} - \mathbf{x}_i| (n_{\text{H I}} \sigma_x)_{\text{prev. cell}}$, and a frequency Lorentz transformed to the bulk velocity of the new cell. This procedure is repeated until either the originally assigned value of τ is spent, and the photon is scattered, or it leaves the computational box.

2.4. Scattering

Except for a small recoil effect, the scattering is coherent in the reference frame of the atom. However, to an external observer, the non-zero velocity $\mathbf{u} = \mathbf{v}_{\text{atom}}/v_{\text{th}}$ of the atom will shift the frequency of the photon. In the directions perpendicular to $\hat{\mathbf{n}}_i$, the velocities $u_{\perp 1,2}$ will follow a Gaussian distribution. When $x \sim 0$, the photon barely diffuses spatially. Only when it has diffused sufficiently far in frequency space, will it be able to make a large journey in real space. To skip these non-important core scatterings and thus accelerate the code, if $|x|$ is less than some critical value x_{crit} , following Dijkstra et al. (2006) $u_{\perp 1,2}$ is drawn from a truncated Gaussian so as to favor fast moving atoms and artificially push the photon back in the wing. x_{crit} is determined according to $a\tau_0$ in the given cell. If $a\tau_0 \leq 1$, a proper Gaussian is used; otherwise we find that $x_{\text{crit}} = 0.02 e^{\xi \ln^{\chi} a\tau_0}$, where $(\xi, \chi) = (0.6, 1.2)$ or $(1.4, 0.6)$ for $a\tau_0 \leq 60$ or $a\tau_0 > 60$, respectively, can be used without affecting the final result. The effect of this acceleration scheme is a speed-up of several orders of magnitude.

Due to the resonance nature of the scattering event, the velocity u_{\parallel} parallel to $\hat{\mathbf{n}}_i$ depends on x , and is generated following Zheng & Miralda-Escudé (2002).

The final frequency x' of the scattered photon (in the reference frame of the fluid element) depends on direction in which the photon is scattered. For scattering in the line center, transitions to the $2P_{1/2}$ state results in isotropic scattering, while the $2P_{3/2}$ transition causes some polarization, resulting in a probability distribution $W(\theta) \propto 1 + \frac{3}{7} \cos^2 \theta$, where θ is the angle between $\hat{\mathbf{n}}_i$ and the outgoing direction $\hat{\mathbf{n}}_f$ (Hamilton 1940). Since the spin multiplicity is $2J + 1$, the probability of being excited to the $2P_{3/2}$ state is twice as large as being excited to the $2P_{1/2}$ state³. For scatterings in the wing, polarization for $\pi/2$ scattering is maximal, resulting in a dipole distribution $W(\theta) \propto 1 + \cos^2 \theta$ (Stenflo 1980). The transition from core to wing scattering is given by the value of x where the Lorentzian starts dominating the Gaussian profile, i.e. where $a/\pi x^2 \sim \sqrt{\pi} e^{-x^2}$, or $x \sim 3$ (the exact value is not crucial). In all cases,

³ For the environments produced here, transitions to the $2S$ state and subsequent destruction of the photon can be neglected.

the scattering is isotropic in the azimuthal angle ϕ . In the observers frame, the final frequency is then given by $x' = x - u_{||} + \hat{\mathbf{n}}_f \cdot \mathbf{u} + g(1 - \hat{\mathbf{n}}_i \cdot \hat{\mathbf{n}}_f)$, where the factor $g = h_{P1}\nu_0/m_Hcv_{th}$ (Field 1959) accounts for the recoil effect.

2.5. Observable Surface Brightness Maps

Following the above scheme, the photons are propagated through the medium, one by one, until they escape the computational box. For each scattering (as well as the emission) of a photon, the probability that the photon will escape in the direction of six virtual observers situated in the negative and positive directions of the three principal axes is calculated. This probability is added as a weight to a three dimensional array (the two spatial dimensions of the projected image of the galaxy, plus a spectral dimension for each pixel). The array is finally collapsed along the spectral dimension and along the spatial dimensions to yield the image and spectrum, respectively, that an external observer would see. The contribution of each pixel element to the surface brightness (SB) is then

$$SB_{\text{pix}} = \frac{L_{\text{tot}}}{n_{\text{ph}}} \frac{1}{d_L^2} \frac{1}{\Omega_{\text{pix}}} \sum_{\text{ph.,scat.}} e^{-\tau_{\text{esc}}} W(\theta), \quad (3)$$

where n_{ph} is the number of photons, d_L is the luminosity distance to the observer, Ω_{pix} is the solid angle subtended by the pixel, and τ_{esc} is the optical depth of the gas lying between the scattering event and the edge of the computational box in the direction of the observer.

The MC code was tested on various simple configurations for which analytic solutions exist, discussed in the introduction. Our code exquisitely passes all tests. The results of these tests will be presented in a future paper.

3. RESULTS

The MC code was applied to a proto-galaxy at $z = 3.6$, consisting of two small, star-forming “disks” separated by approximately 2 kpc, on one of which the computational box is centered, and a third more extended disk of lower star formation rate (SFR), located about 15 kpc from the center. The star-forming regions are embedded in a significant amount of more diffuse, non-star-forming HI gas in a 10–15 kpc thick, sheet-like structure, taken to constitute the x - y plane. The total SFR of the system is $22 M_{\odot} \text{ yr}^{-1}$. Observed LBGs have SFRs in the range 10–1000 $M_{\odot} \text{ yr}^{-1}$ (e.g., Rigopoulou et al. 2006), so the simulated galaxy corresponds to a small LBG. The Ly α emissivity is produced according the three different scenarios described in the introduction. Specifically, the luminosity originating from the HII in the vicinity of massive stars (accounting for approximately 90% of L_{tot}) is determined following Fardal et al. (2001), using the code Starburst99 (Leitherer et al. 1999) to yield the Lyman continuum and assuming a Miller-Scalo initial mass function, a mean Lyman continuum photon energy of 1.4 Rydberg, and that 0.68 Ly α photons are emitted per photonization. The length of the box used for the MC calculations is 50 kpc (physical), and $d_L \sim 34$ Gpc.

Fig. 1 shows the results obtained (all with a resolution of 512^3 cells), viewed from two different directions — from the negative x - and z -direction, corresponding to

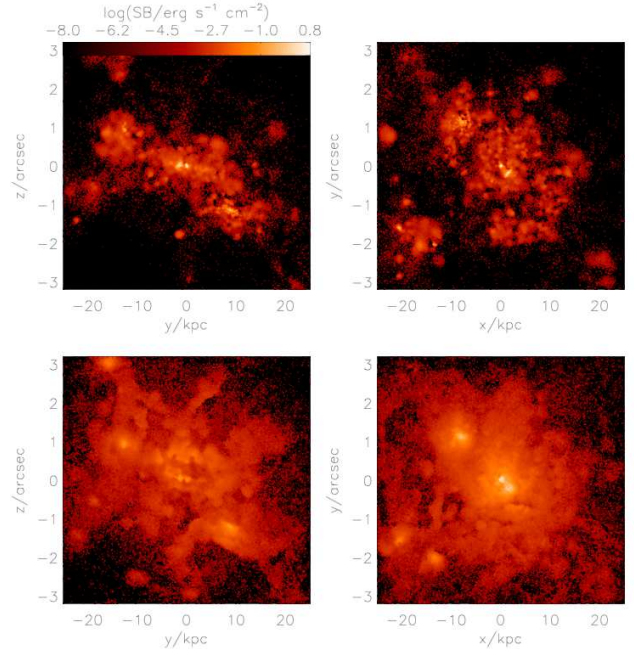


FIG. 1.— Bolometric surface brightness map of a simulated galaxy at $z = 3.6$. Left and right column shows the system when viewed edge-on and face-on, respectively. The top panel displays the galaxy as if the Ly α radiation was able to escape directly, without scattering. The bottom panel shows the effect of the scattering.

an edge-on and a face-on view of the sheet-like structure, respectively. Upper panels assume that the gas is optically thin to the Ly α line, lower show the corresponding results with resonant scattering included.

The effect of the scattering is incontestable: although the original constellation of the principal emitters is still visible, the surface brightness distribution is clearly much more extended. Moreover, we notice the effect of the viewing angle. Qualitatively, we expect the photons to escape more easily from the face of the sheet than from the edge and hence that the system should have a higher surface brightness than when viewed edge-on. Here, this anticipation is quantified: Fig. 2 shows the azimuthally averaged SB profiles. To allow for direct comparison with observations, the profiles are also shown not including the luminosity of the emitter lying in the outskirts of the image and smoothed with a PSF corresponding to a seeing of $0.8''$. The maximum SB of the x - y plane is found to be $6.1 \times 10^{-2} \text{ erg s}^{-1} \text{ cm}^{-2}$, or ~ 14 times higher than that of the y - z plane. The average SB, from which the total luminosity is usually derived assuming isotropic emission, is 3.8 times higher.

Finally, we show the emergent spectrum. Though not as clear for the edge-on view, both profiles exhibit the characteristic double-peaked profile (see, e.g., Venemans et al. 2005). Obviously, this is the result of the high opacity for photons near the line center; diffusing to either side of ν_0 quickly decreases τ so as to make escape more probable. Furthermore, both profiles imply a net inward velocity of the gas; for infalling gas, red photons are shifted into resonance, while blue photons escape even more easily, thus enhancing the blue peak and diminishing the red.

Fitting a “Neufeld profile” to the observed spectra can give us an idea of the intrinsic characteristics of the sys-

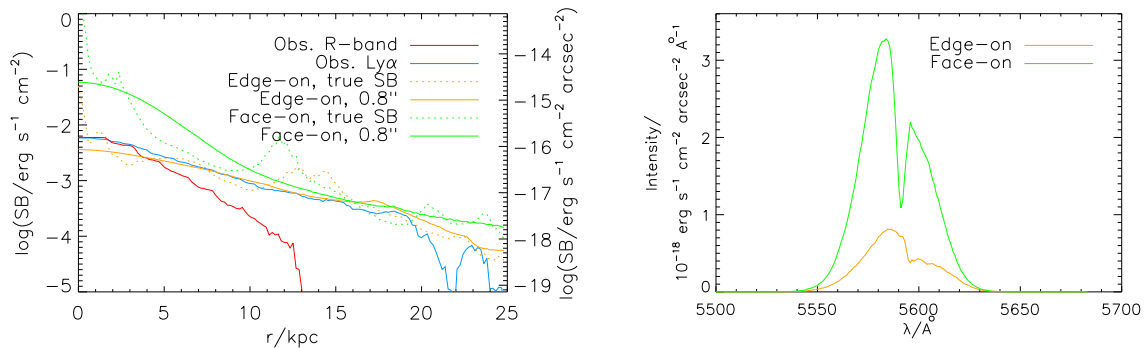


FIG. 2.— *Left*: Bolometric surface brightness (SB) profiles of the galaxy when viewed edge-on (*orange*) and face-on (*green*). Both the true (*dotted*) and the smoothed (*solid*, see text) profiles are displayed. Also shown are the SB profiles of the galaxy LEGO2138.29 (SFR $\sim 15 M_{\odot} \text{ yr}^{-1}$ if extinction is negligible, Fynbo et al. 2003) in Ly α (*blue*) and in the R-band (*red*, normalized to the maximum observed Ly α SB). In particular the SB of the y - z plane nicely reproduces the observed SB. Left axes measure the SB at the source, while right axes measure the SB observed at $z = 0$. *Right*: Spectrum of the emergent radiation, clearly displaying the characteristic double-peaked profile. The enhanced blue peak indicates a net inward bulk velocity of the gas.

tem. Unfortunately, there is a degeneracy in that the profile is dependent only on the parameter $a\tau_0$. Assuming some temperature, e.g. 10^4 K, representative of most of the Ly α emitting gas, one could in principle deduce the equivalent column density N_{HI} . Alternatively, if N_{HI} is obtainable due to, e.g., the presence of a background quasar, constraints can be put on the temperature.

A bulk rotational motion of the gas will also alter the profile. Since in fact a full spectrum is obtained for every pixel element, this effect can be studied through long-slit spectroscopy.

4. DISCUSSION AND CONCLUSION

The present MC calculations do not include the effect of dust. Effectively, dust will act as a photon sink and an extra scattering possibility. Since, on average, each photon scatters $\sim 4 \times 10^8$ times and travel a distance of ~ 40 kpc before escaping (determined from a non-accelerated run of the code with a few 10^3 photons), approximately half of which is in the high density ($n_{\text{HI}} \gtrsim 0.1 \text{ cm}^{-3}$), cooler ($T \sim 10^4$ K) regions, even a small amount of dust may be expected to be capable of causing a significant decrease in the observed intensity. However, it is not clear to which extent the dust will affect the observations. If the medium is clumpy, the ratio of Ly α to continuum radiation may in fact be increased (Neufeld 1991; Hansen & Oh 2006). Moreover, Tasitsiomi (2006) argued that dust acting as catalysator for hydrogen molecules will lower n_{HI} , making the medium more transparent. We will study these effects in future work, implementing a realistic model of the dust based on the 8 different

metal species kept track of by the cosmological simulation.

As a very recent improvement of the cosmological simulation, a post-processed RT scheme of UV radiation from star-forming regions was developed by Razoumov & Sommer-Larsen (2006). They found that up to 5–10% of the ionizing photons escape these regions at $z \sim 3.6$. However, a very preliminar analysis indicates that the results presented in this work are not significantly changed by the inclusion of H-ionizing photon RT. The quantitative effects of this on Ly α RT will also be discussed in a forthcoming paper.

The developed Monte Carlo code has reproduced qualitatively and quantitatively the observation that young galaxies often appear significantly more extended on the sky in Ly α than in the optical. Furthermore, we investigated the impact of the viewing angle on the observed surface brightness. Future simulations of a large statistical sample of galaxies, taking properly into account dust and H-ionizing UV photon radiative transfer, will allow us to learn more about the enigmatic Ly α emitters.

The authors are very grateful to J. Fynbo and T. Haugbølle for beneficial discussions, to A. Tasitsiomi for quick response to questions, and to J. Schaye for useful comments. We also thank the anonymous referee for constructive remarks. The simulations were performed on the SGI Itanium II facility provided by DCSC. The Dark Cosmology Centre is funded by the DNRF.

REFERENCES

- Cantalupo, S., Porciani, C., Lilly, S. J., & Miniati, F. 2005, *ApJ*, 628, 61
Dijkstra, M., Haiman, Z., & Spaans, M. 2006, *ApJ*, 649, 14
Fardal, M. A., Katz, N., Gardner, J. P., Hernquist, L., Weinberg, D. H., & Davé, R. 2001, *ApJ*, 562, 605
Field, G. 1959, *ApJ*, 129, 551
Furlanetto, S. R., Schaye, J., Springel, V., & Hernquist, L. 2005, *ApJ*, 622, 7
Fynbo, J. P. U., Møller, P., & Thomsen, B. 2001, *A&A*, 374, 443
Fynbo, J. P. U., Ledoux, C., Møller, P., Thomsen, B., & Burud, I. 2003, *A&A*, 407, 147
Hamilton, D. R. 1940, *Phys. Rev.*, 58, 122
Hansen, M. & Oh, S. P. 2006, *MNRAS*, 367, 979
Harrington, J. P. 1973, *MNRAS*, 162, 43
Leitherer, C. et al. 1999, *ApJS*, 123, 3
Loeb, R. & Rybicki, G. B. 1999, *ApJ*, 524, 527
Møller, P. & Warren, S. J. 1998, *MNRAS*, 299, 611
Neufeld, D. 1990, *ApJ*, 350, 216
Neufeld, D. 1991, *ApJ*, 370, L85
Partridge, R. B. & Peebles, P. J. E. 1967, *ApJ*, 147, 868
Razoumov, A. O. & Sommer-Larsen, J. 2006, *ApJ*, 651, 81
Rigopoulou, D. et al 2006, *ApJ*, 648, 81
Sommer-Larsen, J., Götz, M., & Portinari, L. 2003, *ApJ*, 596, 47
Sommer-Larsen, J. 2006, *ApJ*, 644, L1
Stenflo, J. O. 1980, *A&A*, 84, 68
Tasitsiomi, A. 2006, *ApJ*, 645, 792
Venemans, B. et al. 2005, *A&A*, 431, 793
Verhamme, A., Schaerer, D., & Maselli, A. 2006, *A&A*, 460, 397

Zheng, Z. & Miralda-Escudé, J. 2002, ApJ, 578, 33